Proc. of SPIE Vol. 2717, Smart Structures and Materials 1996: Smart Structures and Integrated Systems, ed. I Chopra (May 1996) Copyright SPIE

UltraQuiet platform for active vibration isolation

Eric H. Anderson, Donald J. Leo, and Mark D. Holcomb
CSA Engineering, Inc., 2850 West Bayshore Road, Palo Alto, CA, 94303

ABSTRACT

This paper describes an active/passive system designed to provide a stable, isolated platform for vibration-sensitive equipment. The UltraQuiet Platform includes three subsystems: a six-strut, six-axis passive-active vibration isolation mount, a damped support bench, and specialized vibration isolation mounts which reduce transmission of narrowband vibration from individual noisy components on the quiet platform. This paper emphasizes the six-axis Stewart platform active isolation system, which uses a novel series approach to active-passive isolation within each strut. The stiff electromagnetic actuator and geophone velocity sensors in the struts are described. Control design and active vibration isolation performance are summarized. Vibration reduction of up to 20 dB was demonstrated over a 100 Hz bandwidth. Reduction in isolation performance which resulted when the system was mated with a highly flexible base structure is noted.

Keywords: active isolation, structural control, smart structures, narrowband isolation, precision manufacturing, piezoelectrics, Stewart platform

1 INTRODUCTION

As demands for precise positioning increase, there is growing need to provide low vibration environments for instruments, machines, and sensors. Submicron vibration levels are required for applications ranging from semiconductor fabrication to precision machining. The specific motivation for the development of the UltraQuiet Platform (UQP) system (Figure 1) is the requirement to insure steady spacecraft instruments and sensors capable of accurately pointing over long distances. Devices which observe the Earth or its atmosphere, or monitor non-terrestrial objects, can all benefit from steady vibration-free platforms. Although the disturbance environment on-board spacecraft is relatively benign, few built-in dissipation mechanisms are present for reducing vibration. Input forces from components such as solar array drives and reaction wheels are transmitted through the spacecraft bus to produce jitter and errors in instrument pointing. Vibration isolation can limit this transmission.

The STRV-2 spacecraft is one example of a system which will test vibration isolation. A critical instrument planned for this spacecraft is a medium wave infrared (MWIR) telescope designed to track objects in the Earth's atmosphere. The STRV-2 Vibration Isolation, Suppression and Steering system (VISS) will support the MWIR payload.[1] The cryocooler which will be used to cool the telescope is a potentially significant on-platform disturbance force input. Relevant physical parameters from the STRV-2 and other spacecraft helped guide the UQP research. Among these quantities were the payload mass (10–20 kg) and details of the mounting geometry.

While many spacecraft instruments have requirements for both high frequency jitter and low frequency pointing, a decision was made to focus the effort on the reduction of jitter. The amplitude of motion resulting at spacecraft components experiencing vibration is small, in the tens of microns for STRV-2. This low amplitude drove the UQP

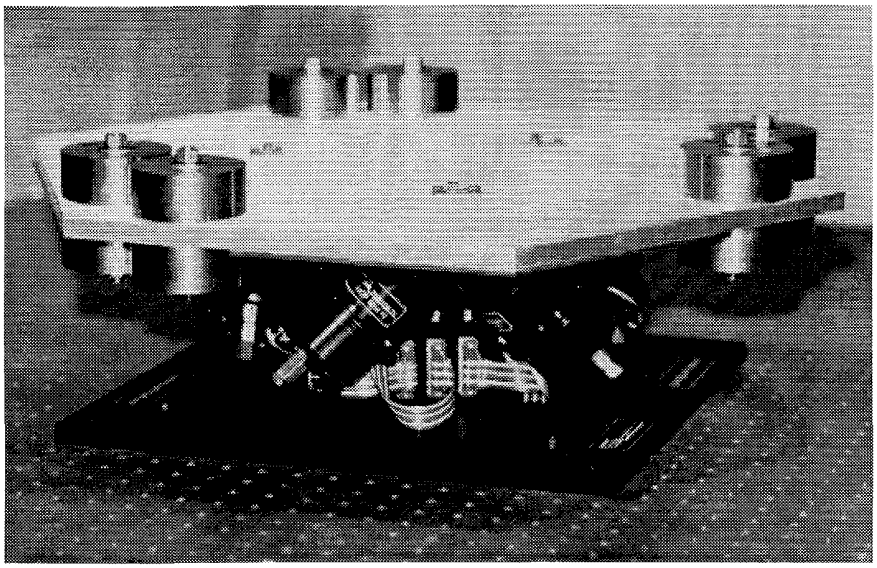

Figure 1: The UltraQuiet Platform (UQP)

design to emphasize precision in actuation, sensing, and control. The research attempted to take novel approaches to development of individual components of the active system. Although the components were intended for the spacecraft platform application, their basic design is transferrable to use on the Earth.

After a note on the approach to active-passive isolation, the paper continues with a discussion of the three major subsystems. The damped platform bench and narrowband component isolation are summarized first. A discussion of the isolator struts which make up the six-strut system follows. Included in that discussion are sections on the electromagnetic sensing and actuation, and on the passive soft mount isolator. The approach to single-axis control is outlined, and the test procedure and test results are summarized. The integrated system, and multi-axis control results on a rigid base structure, are discussed next. Finally, a series of multi-axis control tests carried out with the UQP mounted to a flexible base structure is summarized.

2 APPROACH TO ACTIVE-PASSIVE ISOLATION

One novel aspect of the UQP system is the specific active-passive isolation architecture within each strut. The project goal was to develop a hybrid active-passive vibration isolation system relevant to a range of applications in space and on the Earth. Among these are isolation of semiconductor manufacturing equipment, optical benches, engine mounts, and precision instrumentation. Active isolation certainly offers the possibility of improved performance over purely passive systems. However, some active isolators take poor advantage of built-in passive properties. The more effective approaches to active isolation build on passive characteristics to enhance performance while reducing power requirements. The UQP's main six-axis isolation system and component isolators are each series active-passive hybrids.

Figure 2 illustrates two main classes of active-passive vibration isolators.[2,3] The conventional configuration on the left is a soft active stage in parallel with a soft passive stage. The passive stage can be modeled as a spring and dashpot and the active stage as a feedback control system including a sensor measurement and a control actuator.

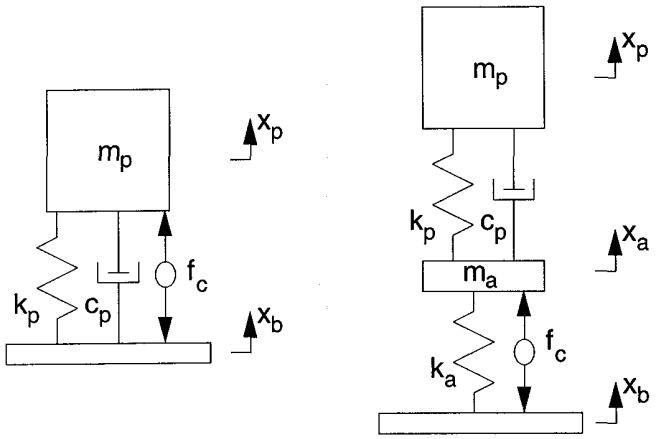

Figure 2: Lumped-parameter models of parallel (left) and series (right) isolators describe components which are designed to reduce the ratio of payload to base motion (x_p/x_b)

The measurement is typically taken directly from the motion of the payload. The less conventional isolator type is a two-stage device consisting of a soft passive isolator in series with a relatively stiff active stage. For this series configuration, the sensor measurement is taken from the motion of the actuator moving mass. That sensor is decoupled from high frequency payload dynamics by the passive isolator. A typical passive mount would be sized to provide a 20 Hz isolation mode frequency. This frequency is high enough to introduce minimal static sag (0.6 mm in a 1-g field).

The total transmissibility across the single-axis series mount is a frequency-domain multiplication of the fixed passive mount transmissibility and the variable active mount transmissibility. The main UQP mount is a six-axis isolation system which was designed to the extent possible to be treated as six series configuration single-axis struts. Use of this configuration implies that the active isolation is predominantly one-directional. Transmission of forces generated on the isolated component is affected only by the passive isolation. Active suppression of vibration originating on the isolated platform using the six struts could be implemented with additional sensors. Each axis of the component isolation designed for vibration-producing devices on the platform acts like an upside-down version of one of the main struts. Devices are isolated so that they are free to move, but the intermediate stage (m_a) motion within each mount and resultant forces transmitted through the mount, are minimized.

3 DAMPED PLATFORM BENCH

The platform bench is the hexagonal structure shown in Figure 1. The damped bench limits detrimental effects of resonances of the isolated payload. It was designed to support payload or instrument while suppressing high frequency vibration originating on or off the platform and acting to reduce flexible coupling and mechanical crosstalk from actuators to sensors in other struts. Natural modes of the lightweight structure were designed to be high in frequency and well damped. Any specific satellite instrument package would likely use a custom support dictated by space constraints or other subsystem requirements. The hexagonal platform selected represents a generic instrument bench. The mass and inertia distributions of the platform with payload simulation masses (thick disks in Figure 1) can be tailored to produce asymmetries representative of specific instruments. In most of the tests, an on-platform mass of 13.2 kg was used in the form of twelve 1.1 kg steel masses. With the 2.9 kg of the damped platform itself, the total isolated mass was 16.1 kg.

Table 1: Modal frequencies for suspension and flexible modes of the undamped UQP

Mode	Freq. (Hz)
XY-rotation	11.4
XY-rotation	11.7
Z-rotation	12.8
XY-translation	19.0
XY-translation	19.0
Z-bounce	24.1
Flex 1	130.1
Flex 2	133.7
Flex 3	134.8

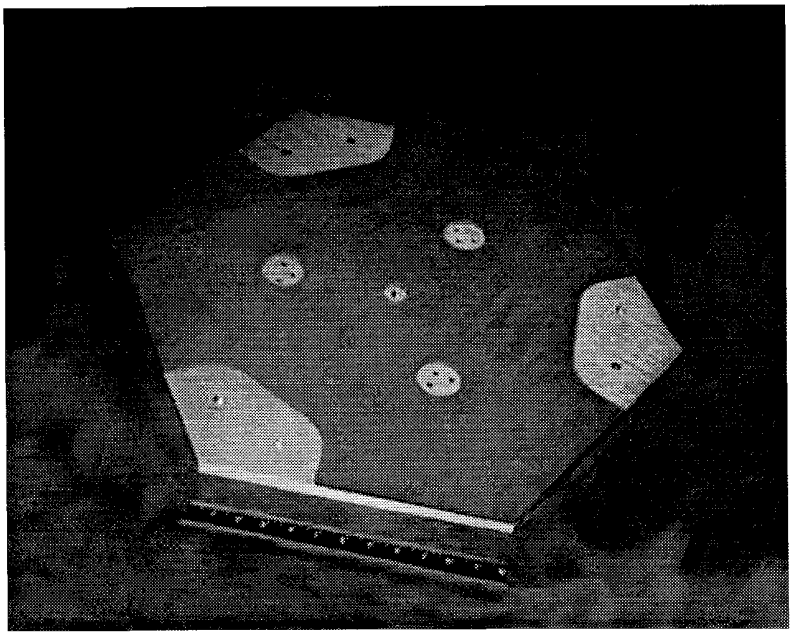

Figure 3: The underside of the damped platform bench shows cutouts for attaching struts and mass simulators

A finite element model was used to design both the platform bench and the passive damping treatment that was applied to it. A nominal distributed payload of 18.2 kg (40 lb) was assumed for the damping design. The goal of the damping treatment was to remove energy from the primary and secondary bending and torsion modes of the panel. The hexagonal aluminum honeycomb panel had dimension 0.61 m (24 in.) across opposing vertices. Struts attached to the platform on a circle of diameter 234 mm (9.2 in.), and the strut bases were mounted on a circle of 330 mm (13.0 in.). Six suspension modes were predicted between 11.4 and 24.1 Hz (Table 1), and the first structural mode was expected at 130.1 Hz.

A constrained-layer passive damping treatment was designed using the modal strain energy approach.[4] This method assumes that the modal damping of a structure may be approximated by the sum of the products of the loss factor of each material and the fraction of strain energy in that material for each mode. The material properties and thickness of both a viscoelastic material (VEM) and a graphite-eopxy constraining layer were optimized. The damping treatment stiffened the lowest frequency flexible modes to 147 Hz, 148 Hz, and 149 Hz, and increased modal damping ratios to greater than 0.05 for the three modes. Figure 3 shows the underside of the completed damped platform. Both the undamped bench, and the bench augmented with passive damping, were used separately in the six-axis active isolation experiments.

4 COMPONENT MOUNTS FOR NARROWBAND ISOLATION

The present UQP architecture does not include the sensors required to allow the main isolation system to reject on-board disturbances. Instead, individual mounts were designed to support noisy components on the nominally-quiet platform. In typical applications, the number of vibration-producing components is likely to be small. On a spacecraft instrument bench, a single cryocooler or scanning device might be present. In other applications, a small number of powered devices could generate disturbance forces. In many instances, the character of the disturbance forces generated is narrowband, and the disturbance energy is concentrated in one or several narrow frequency bands.

The physical mounts developed for the component isolation were series active-passive devices with the piezoelectric active stage nearer the vibration-producing component. These mounts are capable of either broadband or narrowband isolation depending only on the control approach used. Figure 4 illustrates a test conducted to demonstrate narrow-band vibration isolation in two axes. A spinning motor with a small mass eccentricity provided the disturbance force input. The eccentric rotation resulted in two axes of forces. The motor assembly was flexured with soft springs in the vertical direction. In the two horizontal directions, elastomeric mounts provided isolation with corner frequencies above 50 Hz.

Inputs to the active piezoelectric stages of the two mounts were determined based on measured acceleration at the intermediate stage (m_a in Figure 2). Independent channels of LMS adaptive control operated on each mount. the convergence time was varied depending on the desired frequency tracking rate. A resolver on the motor provided a means of tracking the rotation rate as it was varied from 1500 rpm to 2400 rpm (25 Hz to 40 Hz). Figure 5 shows the measured 35 dB reduction in acceleration measured at one mount at the 31.1 Hz operating frequency used in that test. Though the transmitted force was not measured directly, the reduction should be commensurate with the acceleration attenuation. Reduction in the second mount for this case was less (23 dB). In all cases, there was some higher harmonic distortion attributed to nonlinearities in the piezoelectric actuators.

5 SIX-AXIS ISOLATION MOUNT

Six identical struts or mounts comprise the main Stewart platform. The geometrical arrangement of the struts can be varied to accommodate different payloads, geometries, masses, and inertias. The configuration which was selected in this effort represents a point design tailored to a specific payload. Table 2 lists several key strut properties.

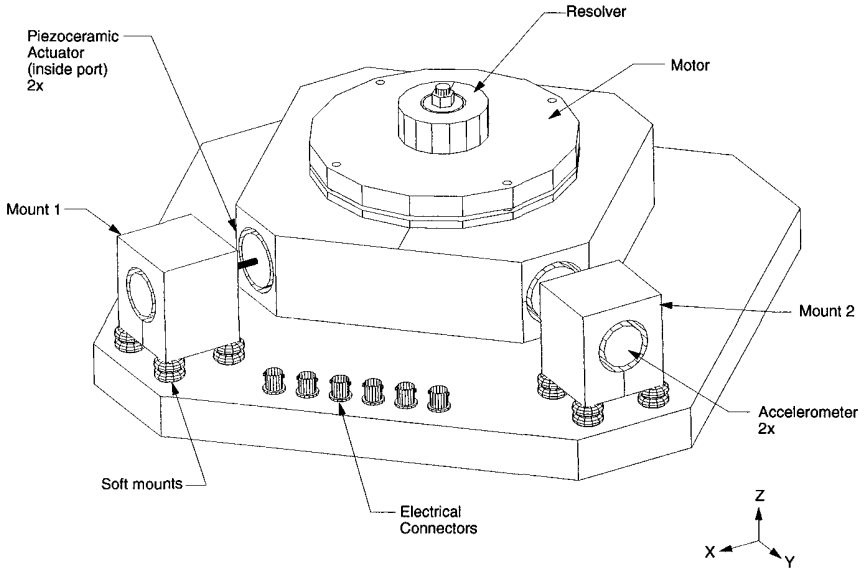

Figure 4: Test setup for evaluation of two-axis narrowband isolation

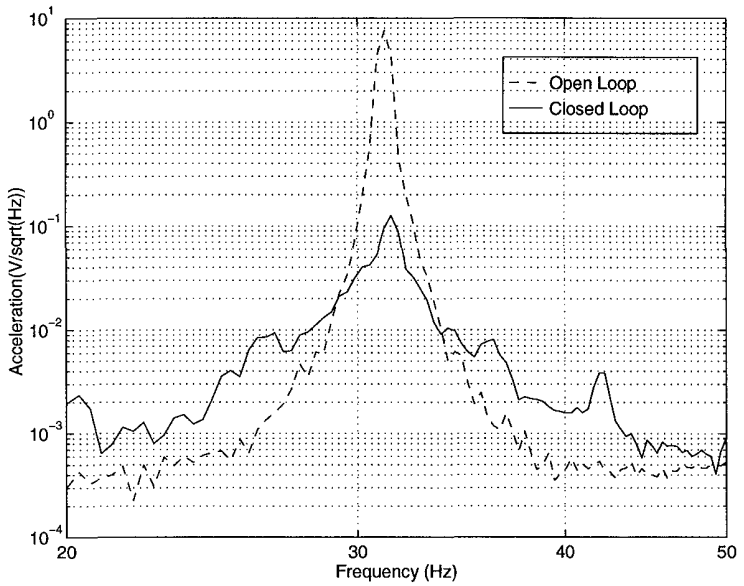

Figure 5: Measured acceleration response on base side of one mount with LMS control

Table 2: Summary of isolator strut properties

Property	Value
Mass	1.1 kg
Force capacity	55 N
Stroke capacity	20 μm
Power (Peak)	5 W

Table 3: Main technical issues addressed during development

Item	Concerns	How resolved
Actuator response	Fidelity for small motion (< 1 mil), nonlinearities, electronic noise	Stiff spring restricts motion
Sensor resolution/noise	Requirement to resolve submicron motion at low frequency	Ganged sensors, local conditioning, variable gain
Kinematic mounts	Need to eliminate mechanical crosstalk, minimize stiction, backlash	Flexures, tolerance checks
Performance validation	Low frequency, low motion, multiple axes	Seismic accelerometers, multiple test sets
Space qualifiability	Damping materials, mass	Materials database, detailed modeling

The amount of stroke is adequate for the spacecraft jitter reduction application considered. Power consumption includes both energy dissipated in the strut and consumption in the amplifier. The following sections describe the actuators, sensors, passive isolators, and other components. Several of the main technical challenges addressed during the development are summarized in Table 3, and a general schematic of an individual strut is shown in Figure 6.

5.1 Actuators

The series isolation architecture requires a stiff actuator. Prototype struts were built using both piezoelectric and equivalent electromagnetic actuators. The electromagnetic actuator eventually selected and refined for the six-axis system was designed to behave as a stiff displacement source rather than a soft force generator. This was accomplished by constraining a force actuator to act against a stiff spring. Since the actuator force generated is proportional to the square of the applied B-field, a bias or offset field must be included to allow a nearly linear response. In the present system, a permanent magnet supplies that field. For small excursions, AC fields created by a time-varying electric current produce an approximately linear force response.

An internal actuator spring is required to limit actuator stroke. Given a force capacity of the electromagnetic actuator, the spring stiffness (k_a) determines stroke capacity according to the simple equation

$$\delta_{act} = \frac{F_{act}}{k_a} \tag{1}$$

The stroke capacity of the present design could easily be doubled by halving k_a. Belleville springs were determined

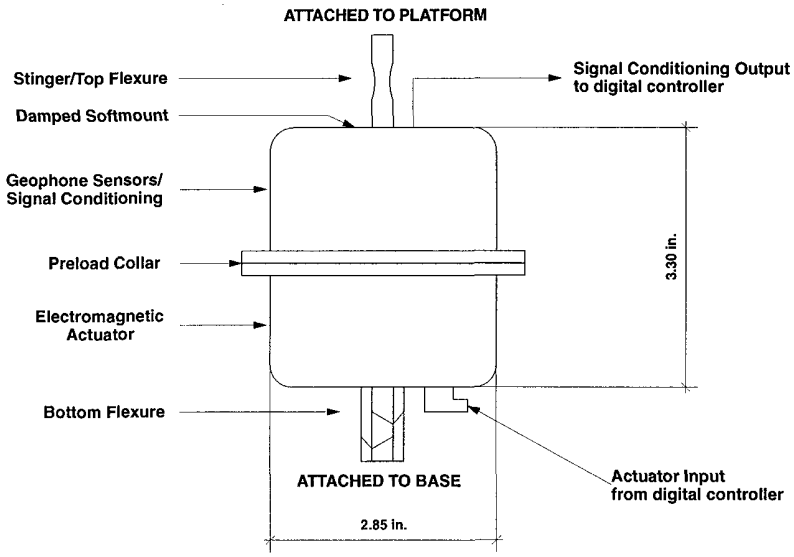

Figure 6: Schematic of a UQP isolator strut

to be the best of several design options considered. The combination of magnetic preload and parallel mechanical preload insured proper registration of individual parts in the final actuator assemblies.

The magnetic actuator assembly was modeled in detail to predict force capability. A boundary element computer model allowed careful estimation of the magnetic B-field in response to changes in the actuator geometry, particularly reduction of material in the dense upper and lower actuator bodies. As the design progressed, the same force capability was retained while mass was trimmed and the field in the magnetic circuit was repeatedly evaluated to guard against saturation. The axisymmetric model was developed with the software package MAGNETO,[5] which was used to calculate fields and forces given permanent magnet (DC) and current (AC) inputs. The model predicted a force of 55 N for the maximum input level of 150 Amp-turns.

Tests to characterize the actuators made use of a custom-built low friction transmissibility tester (Figure 7). The frequency of the internal actuator mode was measured to be 600 Hz, with a Q of 10–15. It was therefore well outside the main active isolation bandwidth (1–100 Hz).

5.2 Sensors

Nominally identical sensor packages were integrated into each of the six struts. The transducer at the core of the sensing subsystem is a geophone. This sensor type was selected after investigation of other sensors, including accelerometers. The reasons for using geophones included relatively high sensitivity and low noise characteristics at low frequency, ruggedness, possibilities for application in active isolation systems on the ground, and low price. Each geophone consists of a mass attached to a single-axis spring supported by the sensor casing. A coil is made part of the moving mass, while a permanent magnet is affixed to the casing. The voltage recorded at the coil's terminals is a function of the coil velocity with respect to the magnet and is also a function of the magnetic field.

$$\frac{\text{Voltage}}{\text{Velocity}} = \frac{Gs^2}{s^2 + 2\zeta_s\omega_s s + \omega_s^2}, \tag{2}$$

where G is the sensor's transduction constant, for example in Volt/(m/s), ω_s its resonant frequency and ζ_s its damping ratio.

Transduction increases with the magnetic field inside the coil, and with the number of coil windings. Larger geophones possess larger transduction constants because they have larger coils and more efficiently used B-fields. The geophone resonance determines the frequency at which the sensor responsivity becomes high. Low frequency responsivity is increased by using a lower sensor resonance. Note, however, that the proof mass inside the geophone sags under gravity by an amount equal to g/ω_s^2, where g is the Earth's gravity.

The UQP isolators use the GS-14 from OYO Geo Space, a compact sensor (17.3 mm high, 15.9 mm in diameter) with a resonance at 28 Hz. The gravity induced sag is 0.32 mm, while the mass can travel 2.3 mm (7 times as far); thus the there is no significant orientation limitation. Its transduction constant is high at 24 Volt/(m/s). Increased sensitivity at low frequency could be realized with a larger geophone, for example the GS-11D, which is 33.5 mm high, 31.8 mm in diameter, and has a resonance at 4.5 Hz, 8 Hz, 10 Hz or 14 Hz. That sensor would not work effectively in both 1-g and 0-g fields because of sag. It might, however, be possible to use two different sensor sets for ground testing and flight operation.

In each strut, six geophones are conditioned to provide a single measurement of motion. The alternating polarization of the geophones allows nominal cancellation of the effect of axisymmetric magnetic field variation. A conditioning circuit within each strut provides an amplified sensor signal and further cancellation. This capability is valuable in tailoring the sensor response to produce a large voltage output for substantial (10 times) differences in base vibration level ranges. Because of the sensor ranging capability, the actuator stroke capacity sets an upper limit on the amount of motion which can be rejected by the isolators.

Low frequency measurement noise ultimately limited performance of the UQP system. The equivalent RMS motion above 0.1 Hz due to electronic amplifier noise was calculated to be 2.6 μm, though equivalent RMS motion above 1 Hz was estimated at only 13 nm. A lower resonance geophone could have eased this noise constraint, at the cost of added size, mass, and static sag.

5.3 Passive Soft Mount Isolator

Each strut is a combination active-passive isolator, with the active and passive stages in series. The passive stage is located between the active stage and the payload. In the absence of power, the passive stages of the six struts provide six axes of isolation. Desirable passive mount features include predictable stiffness, low mass, insensitivity of properties to preload, and controlled material properties. The small displacements faced by the softmount make a flexure type isolator practical.

The flexured softmounts were designed to provide an overall bounce frequency of 20-25 Hz for the UQP mass of 18 kg, with a mechanical Q for all six suspension modes of 5–10. The design was constrained to fit within the diameter of the actuator to avoid impacting overall strut diameter. Other design constraints included stress and cubic stiffening effects due to either static or dynamic deformation. The six-legged flexure was designed iteratively using a finite element model with the material thickness determined based on the frequency constraint. The flexure is clamped in six places along the outer diameter of the mount. The load path is through the flexure to the central pickup point to which the stinger is attached. The modal strain energy method was used to arrive at an optimum viscoelastic material (VEM) for sandwiching between two metal facesheets.

The final configuration has 0.025 in. thick face sheets and 0.005 in. thick VEM. The static stiffness of the flexure in vertical direction was calculated to be 0.185N/μm (1060 lb/in). A static sag of 0.36 mm (14.2 mils) was computed. The predicted mechanical Q at 28 Hz was just under 8. Flexure facesheets were machined in batch from 25-mil Be-Cu stock using an electrical discharge machining (EDM) process. Each flexure was tested to measure stiffness and damping properties. The six flexure stiffnesses ranged from 0.19 N/μm to 0.22N/μm, and measured values of Q ranged from 4.5–6.5.

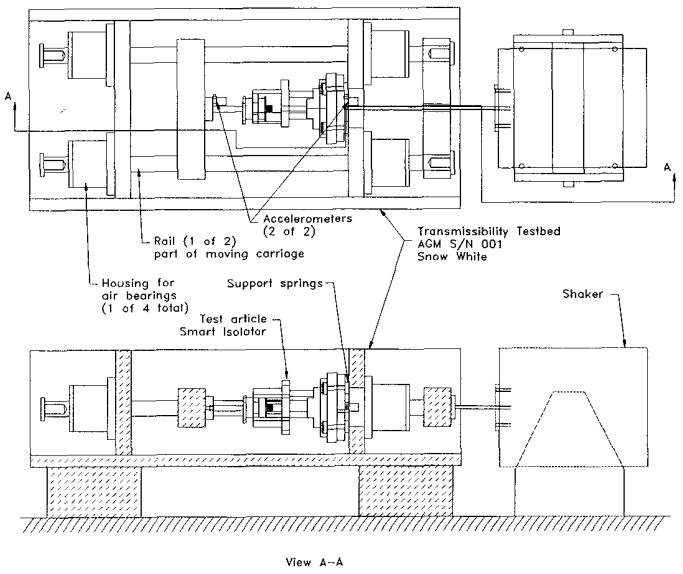

Figure 7: Low-friction single-axis transmissibility tester

5.4 Integrated Six-Axis System

Two sets of three end fittings each were used to mate the six struts with a 0.5 inch thick base plate and damped platform. The smaller upper end fittings bolted in three places to the platform and were threaded to allow bolting of the upper ends of the strut stingers. The larger lower end fittings mate the lower cross-blade flexures to the solid base plate. The plate served as a convenient mechanical interface to a rigid work plate and to a flexible truss.

A three-part electronics interface housing was installed beneath the platform and within the space bounded by the six struts. Its aluminum chassis is of a unique shape designed to take advantage of the available volume. This chassis routs external power, actuator, and sensor signals to the six struts. Three MS connectors on the front of the housing carry ± 12 V power used for the sensor conditioning, the conditioned sensor output headed to the control computer, and the actuator drive signals from the six linear amplifiers. All the sensor and actuator power is provided from an 18–36 Volt bus.

Both digital and analog controllers were implemented on the prototype isolators. A digital system was selected for the full six-axis system for several reasons: ease of use compared to analog systems; compatibility with a space-ready system under development;[6] flexibility in reconfiguring the compensator characteristics; and, trends towards increasing performance per cost in DSP-based systems.

A controller based on the TI TMS320C31 DSP was used. This 33 MHz system was adequate to perform the number of floating point operations required (up to 54-state decoupled linear controller at a 2.5 kHz sampling rate). The system as configured by CSA included a motherboard housing the DSP, six 12-bit A/Ds and D/As, and an AC/DC converter which provided the controller +5V and ± 12V from wall power input. C-code was developed on a 486 PC, compiled, and downloaded to the real-time processor over a serial link. Much of the C-code was generated using custom Matlab routines.

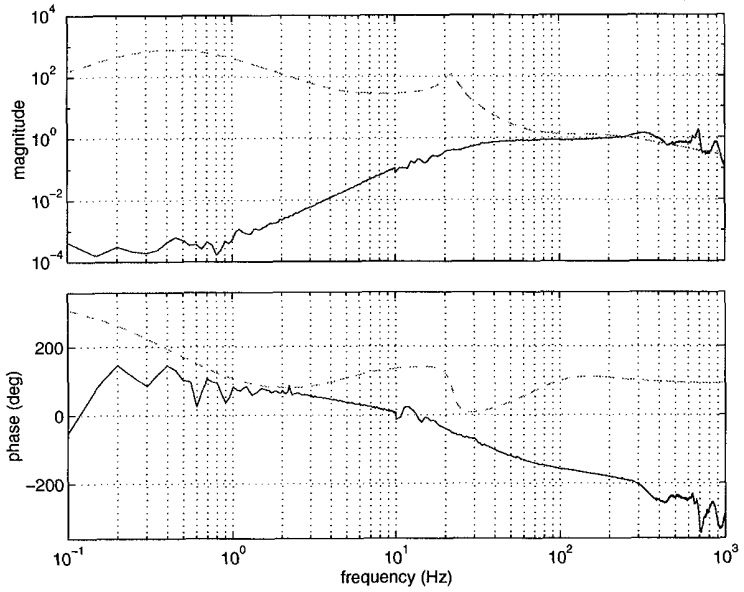

Figure 8: Bode plot of typical single-axis compensator design (dashed) and open loop plant transfer function (solid)

6 CONTROL DESIGN AND TESTS RESULTS

Three sets of tests were conducted. In the first set, individual struts were tested in the low-friction transmissibility tester (Figure 7). The other test sets measured the full six-axis system on either a rigid or flexible base. The mechanical design and isolation architecture allowed the single-axis strut results to carry over almost directly to the Stewart platform system.

Figure 8 is a magnitude and phase plot of the open-loop transfer function measured for one strut between the input voltage to the actuator and the output of the sensor. At frequencies below 1 Hz, the signal is highly corrupted and is essentially in the noise floor at approximately 0.1 mV. Between 1 and 8 Hz, the magnitude rises with a slope of between 40 and 60 dB/dec, which decreases to approximately 40 dB/dec at 8 Hz due to an LR actuator pole. These low frequency dynamics were only obtained after careful adjustment of the sensor signal conditioning. The highly-damped second-order pole at approximately 28 Hz is due to the break frequency of the geophones. The transfer function levels off above this frequency until the actuator dynamics begin occurring at 330 Hz. The open-loop transfer function also exhibits the phase loss associated with the actuator and sensor dynamics. The 90° lag that occurs below 10 Hz is due to the LR pole; the 180° lag that occurs in the mid frequencies is associated with the geophone sensor dynamics. The phase excursions at high frequencies (above 300 Hz) are due to the actuator dynamics. Overall, the open-loop transfer function has a 270° phase lag between 3 and 300 Hz.

A notable characteristic of this transfer function is the lack of observability of the 22 Hz payload bounce mode. This feature is typical of series configuration mounts. It results from an actuator stiffness large compared to the passive stage impedance. As discussed below, this unobservability of the payload bounce mode had ramifications for the compensator design. Since the 'natural' increase in gain did not occur in the open-loop transfer function, it was necessary to add extra dynamics to the compensator to reduce the peak at 22 Hz.

Closed-loop results for several-micron base motion are shown in Figure 9. Active attenuation begins at 8 Hz, with 0.707 attenuation reached at 9 Hz. This is a factor of four improvement over the passive system. The high compensator gain at 22 Hz, and substantial phase margin at high frequencies results in a smooth closed-loop transmissibility that

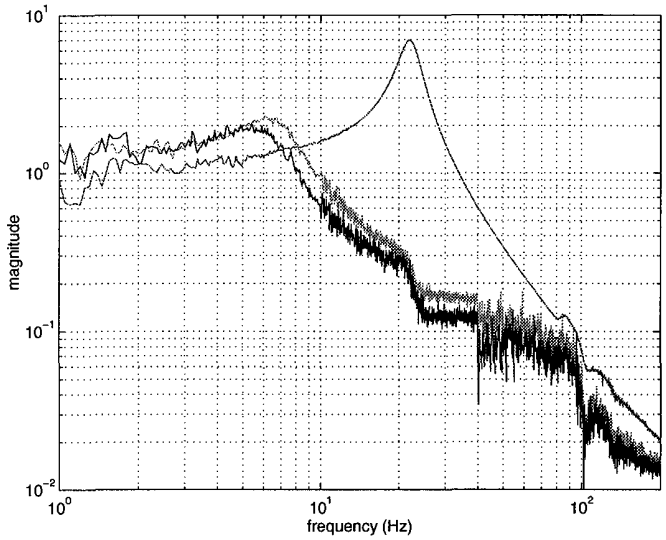

Figure 9: Measured open-loop and closed-loop transmissibility (at two separate gains) for single-axis compensation

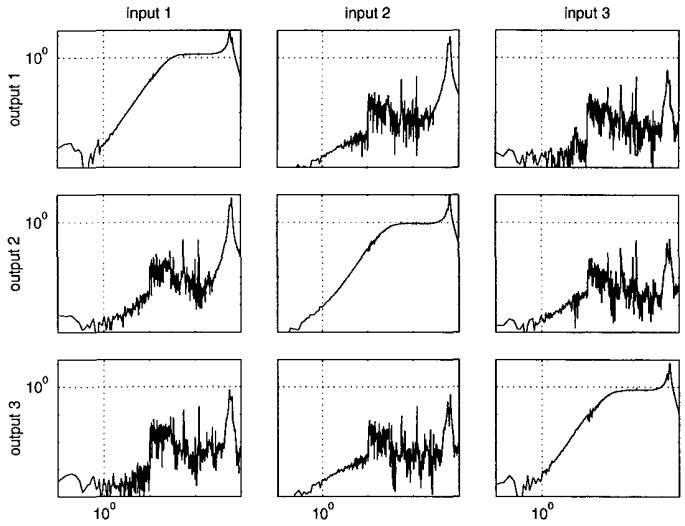

Figure 10: Upper left partition of the 6-by-6 open-loop transfer function matrix between the actuator inputs and the conditioned outputs on rigid base

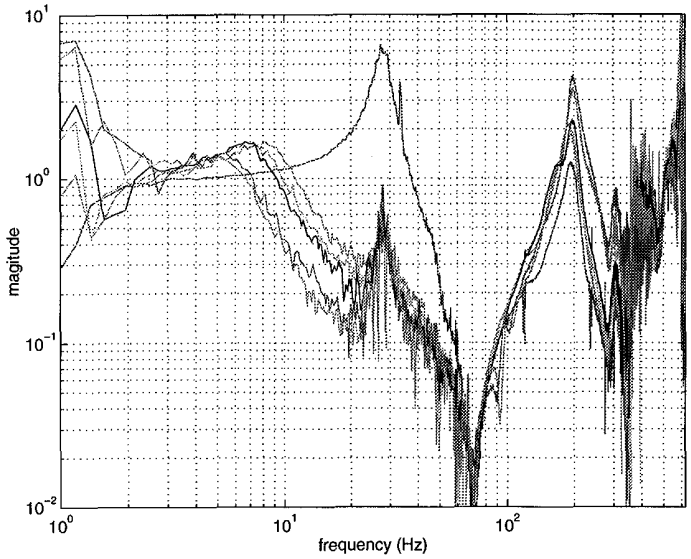

Figure 11: Open-loop and closed-loop transfer function between base accelerometer and center platform accelerometer for five increasing gains for the platform mounted on the workplate

rolls off at approximately a slope of –20dB/decade above 8 Hz. A factor of ten reduction in the transmissibility occurs at approximately 40 Hz, a five times improvement over the purely passive strut.

The single-axis SISO compensator design formed the basis for the MIMO design on the multi-axis isolation system. The matrix of transfer functions between the six actuators and six sets of geophone sensors was obtained for the multiaxis isolation system placed on a large, rigid workplate. One 3 × 3 partition of the transfer function matrix is shown in Figure 10. The passive mount in series with a stiff active stage causes substantial cross-axis decoupling in the multiaxis platform. The on-diagonal transfer functions – the ones between the actuator inputs and their collocated sensor outputs – are almost identical to the single-axis plant transfer function (Figure 8). The payload dynamics that occur in the frequency range 10-30 Hz are not present in the collocated transfer functions, signifying that the open-loop plant transfer functions are insensitive to the payload dynamics. Furthermore, the magnitudes of the off-diagonal transfer functions are at least an order of magnitude less than the magnitudes of the diagonal terms between approximately 3 Hz and 500 Hz, indicating that the system exhibits weak coupling between the multiple inputs and outputs.

The MIMO control design for the multiaxis isolation system was a diagonal set of SISO control laws. The frequency response between the collocated sensor-actuator pair on strut 1 was used to design an 8^{th}-order SISO compensator. The gain of the compensator was scaled such that the loop gain of each on-diagonal term of the series connection of the controller and open-loop transfer matrix was equivalent at 100 Hz. The only significant difference between the single-axis compensator and the MIMO design was the increased rolloff at high frequencies; increased rolloff was necessitated by the light damping in the actuator mode at approximately 600 Hz.

The multiaxis controller was implemented and a closed-loop transfer function was measured between accelerometers located on the base plate and in the center of the platform. The excitation source was a mass-loaded shaker placed on the workplate in close proximity to the isolation system. The closed-loop result is shown in Figure 11. The ratio of motion between the center of the baseplate and the center of the platform is similar to the results for the single-axis tests. Because the response at the platform's center has a negligible component of rotation, this measurement is essentially the transmissibility between the up-and-down translation of the base and the up-and-down translation of the platform. The peak reduction in transmissibility occurs in the range 20-30 Hz, near the translational bounce

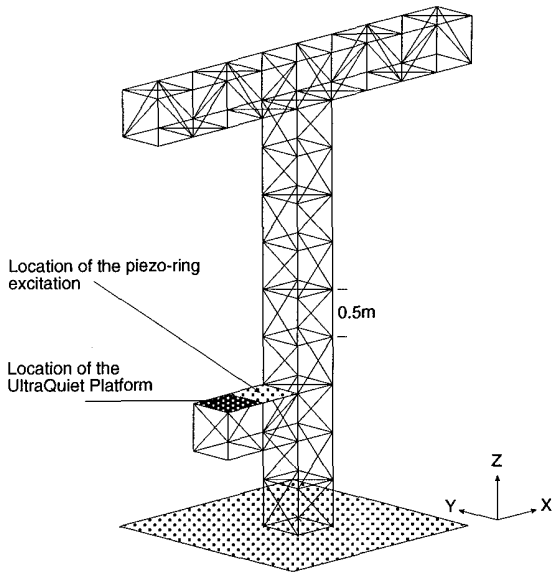

Figure 12: Schematic showing location of prototype UltraQuiet Platform mounted on the flexible T truss

frequency of the platform where the loop gain is highest. The large peak at approximately 200 Hz is a flexible mode of the platform. The response due to flexibility results because gain crossover occurs near the resonant frequency of the platform.

A final set of control tests was performed with the UQP mounted on a flexible appendage of a large truss structure. The main structure was a T truss constructed from aluminum tubing with first mode frequency of 5 Hz. The platform and isolation system were placed on the far bay of a two-bay appendage mounted close to the fixed end of the truss (see Figure 12). The tests used a version of the hexagonal honeycomb platform bench which did not incorporate damping augmentation. A mass-loaded piezoelectric shaker was placed on the adjacent bay to provide a controllable excitation source.

Base flexibility caused increased coupling in the diagonal transfer functions of the open-loop transfer matrix. A comparison of the collocated frequency response for the rigid-mounted UQP and the truss-mounted UQP is shown in Figure 13. The reduced impedance of the base causes pole-zero pairs to appear between 8 Hz and 30 Hz. The pole-zero combinations cause magnitude and phase excursions as compared to the frequency response of the rigidly-mounted platform.

A diagonal set of SISO compensators, similar to those described above, was also implemented on the truss-mounted platform. The piezo-ring shaker excited the truss and the transfer function from an accelerometer placed on the center of the platform and one placed on the base was measured. (Figure 14) The gain of the control law was increased until instability occurred. For the truss-mounted platform, the gain could only be increased to 65% of the full gain when the platform was mounted on the workplate. The reduced gain resulted in a corresponding decrease in performance. Only a factor of ten reduction was achieved near the bounce frequency for the platform mounted on the T truss, as compared to a factor of fifteen reduction achieved with the platform mounted on the workplate.

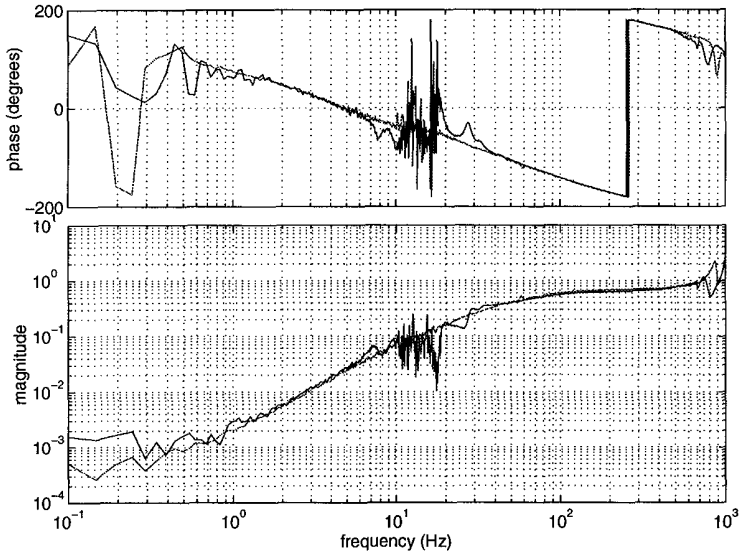

Figure 13: Collocated magnitude and phase for strut 1 for the UQP mounted on the truss and the UQP mounted on the workplate. The flexible truss couples the suspension dynamics into the collocated measurement.

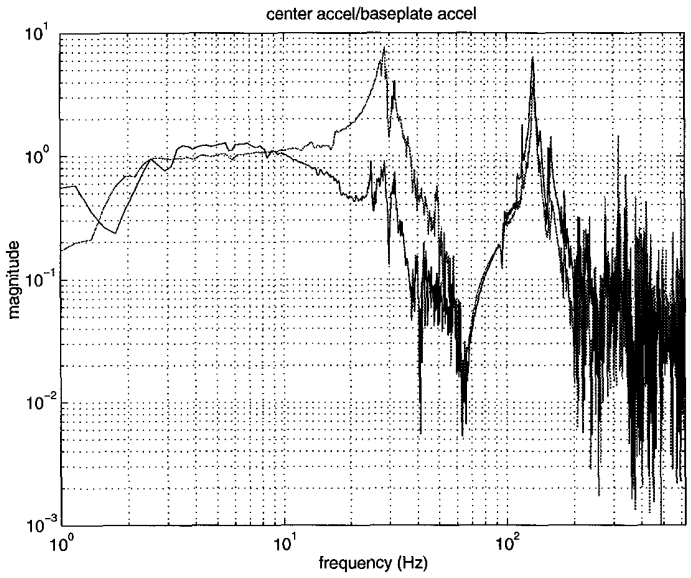

Figure 14: Open-loop and closed-loop transfer function between base acceleration and the acceleration of the center of the platform for the platform mounted on the T truss

7 CONCLUSIONS

A three-part vibration suppression system called the UltraQuiet Platform (UQP) was developed. The UQP is intended to provide an extremely low vibration environment for precision instruments, sensors, and machines. It includes a Stewart platform supporting a damped instrument bench, which in turn supports individual component isolators. This paper describes the UQP, emphasizing the six-axis active-passive isolator mount. A combination stiff electromagnetic actuator and geophone velocity sensors allowed improvement of up to 20 dB in isolation capability with the active system. Performance was limited at low frequency by measurement noise. The system performance was also reduced some when the mount was attached to a highly flexible base. The lowest frequency modes of the support bench were increased passively to above 5% of critical. Narrowband component isolators were effective at reducing force transmission from a rotating device which including a mass eccentricity.

The development was initially motivated by pointing and jitter requirements for spacecraft sensors. Measures were taken to emphasize spaceflight qualifiability whenever possible in the course of the development. Considerations included material selection, susceptibility to stress under launch loads, and remote interfacing. Several aspects of the present system must be addressed prior to flight. It is expected that specific subcomponents will be upgraded to flight standards without radical changes to the basic design.

8 ACKNOWLEDGEMENTS

This work was sponsored by the BMDO through the Small Business Innovation Research (SBIR) program. The contract was administered by the Air Force Phillips Laboratory, with Lt. Michelle Kazmier as Technical Monitor. The authors gratefully acknowledge the contributions of Andreas von Flotow and Hood Technology Corp. in the configuration definition, actuator and sensor design, and prototype development.

9 REFERENCES

[1] Sullivan, J., Hoffman, T., Das A., Davis, P., "Design of a 6 DOF Vibration Isolation System Using Hybrid D-Strut Technology," 19th Annual AAS Guidance and Control Conf., Breckenridge, CO, Feb., 1996, Paper No. 96-062.

[2] Beard, A.M., von Flotow, A.H., and Schubert, D.W., "A Practical Product Implementation of an Active/Passive Vibration Isolation System," SPIE, July 1994.

[3] Leo, D. L. and Anderson, E. H., "Comparison of Multi-Axis Active Vibration Isolation Architectures", ASME Winter Annual Meeting, San Francisco, November, 1995.

[4] Johnson, C.D., and Kienholz, D.A., "Finite Element Prediction of Damping in Structures with Constrained Viscoelastic Layers," *AIAA Journal*, Vol. 20, No. 9, September 1982.

[5] Integrated Engineering Software, 46-1313 Border Place, Winnipeg, Manitoba, Canada R3H 0X4.

[6] Bronowicki, A.J., Innis, J.W., Casteel, S., Dvorsky, G., Alvarez, O.S., Rohleen, E., TRW Space and Technology Div., "Active Vibration Suppression using Modular Elements," SPIE Conference on Smart Structures and Intelligent Systems, Feb., 1994, Paper No. 2190-67.